Journal of Applied Research and Technology
ISSN: 1665-6423
jart@aleph.cinstrum.unam.mx
Centro de Ciencias Aplicadas y Desarrollo Tecnológico
México

Jaime-Acuña, Oscar E.; Villavicencio-García, Humberto; Vázquez-González, Rogelio; Petranovskii, Vitalii; Raymond-Herrera, Oscar

Synthesis of nanostructured metal–, semiconductor–, and metal/semiconductor–mordenite composites from geothermal waste

Journal of Applied Research and Technology, vol. 14, núm. 4, 2016, pp. 232-238
Centro de Ciencias Aplicadas y Desarrollo Tecnológico
Distrito Federal, México

Available online at www.sciencedirect.com

Journal of Applied Research and Technology

Journal of Applied Research and Technology 14 (2016) 232–238

www.jart.ccadet.unam.mx

Original

Synthesis of nanostructured metal–, semiconductor–, and metal/semiconductor–mordenite composites from geothermal waste

Oscar E. Jaime-Acuña [a,*], Humberto Villavicencio-García [b], Rogelio Vázquez-González [c], Vitalii Petranovskii [b], Oscar Raymond-Herrera [d]

[a] *Centro de Investigación Científica y de Educación Superior de Ensenada – Centro de Nanociencias y Nanotecnología-Universidad Nacional Autónoma de México, Ensenada, Baja California, Mexico*

[b] *Centro de Nanociencias y Nanotecnología, Universidad Nacional Autónoma de México, Km 107 Carretera Tijuana-Ensenada, CP 22860, A.P. 14, Ensenada, Baja California, Mexico*

[c] *Departamento de Geofísica de Exploración, Centro de Investigación Científica y de Educación Superior de Ensenada, Carretera Ensenada-Tijuana No. 3918, Zona Playitas, CP 22860, A.P. 360, Ensenada, Baja California, Mexico*

[d] *Centro de Nanociencias y Nanotecnología, Universidad Nacional Autónoma de México, Km 107 Carretera Tijuana-Ensenada, CP 22860, A.P. 14, Ensenada, Baja California, Mexico*

Received 4 September 2015; accepted 31 May 2016

Available online 3 July 2016

Abstract

Successful synthesis of metal–, semiconductor–, and metal/semiconductor–mordenite nanocomposites, using geothermal solid waste as precursor is reported. Powders of nanostructured composites, consisting of metal and/or semiconductor nanoparticles grown on a mordenite-type zeolitic matrix surface, were synthesized by a one-step solvent-free and organic template-free process. The developed methodology is capable of controlling and tuning the final properties of composites from their synthesis and is also reproducible and repeatable. For comparison and demonstration of the application of the final products, dye photocatalysis degradation tests were done using commercial TiO_2 as reference (degradation reached ~75% in 215 min, $k = 0.004\ min^{-1}$), [M]–S–MOR samples revealed better performance (≥95% in 100 min, $k = 0.009\ min^{-1}$).

Keywords: Organic pollution remediation; Multifunctional nanocomposites; Aqueous synthesis; Photocatalysis; Geothermal waste remediation

1. Introduction

Contemporary chemical industries are searching for new techniques that reduce manufacturing costs and mitigate environmental impact. Processes without emissions and free of risky chemicals have therefore become a challenge for researchers, technologists and engineers (Ambec, Cohen, Elgie, & Lanoie, 2013). The lagoon of mineralized waters at the Cerro Prieto geothermal plant, in Mexicali, Mexico (Fig. 1a), is an excellent source of silicon; in an area of approximately 12.5 km^2, it is located between 115°12′ and 115°18′ west longitude and between 32°22′ and 32°26′ north latitude, 36 km away from Mexicali city. Beside the process of geothermal energy conversion, the saturated silica water is conducted to the precipitation lagoon to separate the silica residues from the reinjection water. The silica salts precipitate as amorphous silica, which is used in this work.

On the other hand, porous materials have potential applications in the chemical industry; likewise, the inclusion of transition metals and/or semiconductors into matrices to modify their properties has gained importance for the development of convenience materials (Bibby & Dale, 1985; Cooper et al., 2004). In the field of porous nanostructured materials, zeolites have been applied in areas such as catalysis, water treatment, H_2 production, among others (Zaarour, Dong, Naydenova, Retoux, & Mintova, 2014).

In this work, nanostructured composites based on metal, semiconductor or metal/semiconductor nanoparticles were grown on a mordenite-type zeolite matrix from geothermal

* Corresponding author.
E-mail address: o.jaime.acuna@gmail.com (O.E. Jaime-Acuña).

Peer Review under the responsibility of Universidad Nacional Autónoma de México.

http://dx.doi.org/10.1016/j.jart.2016.05.006

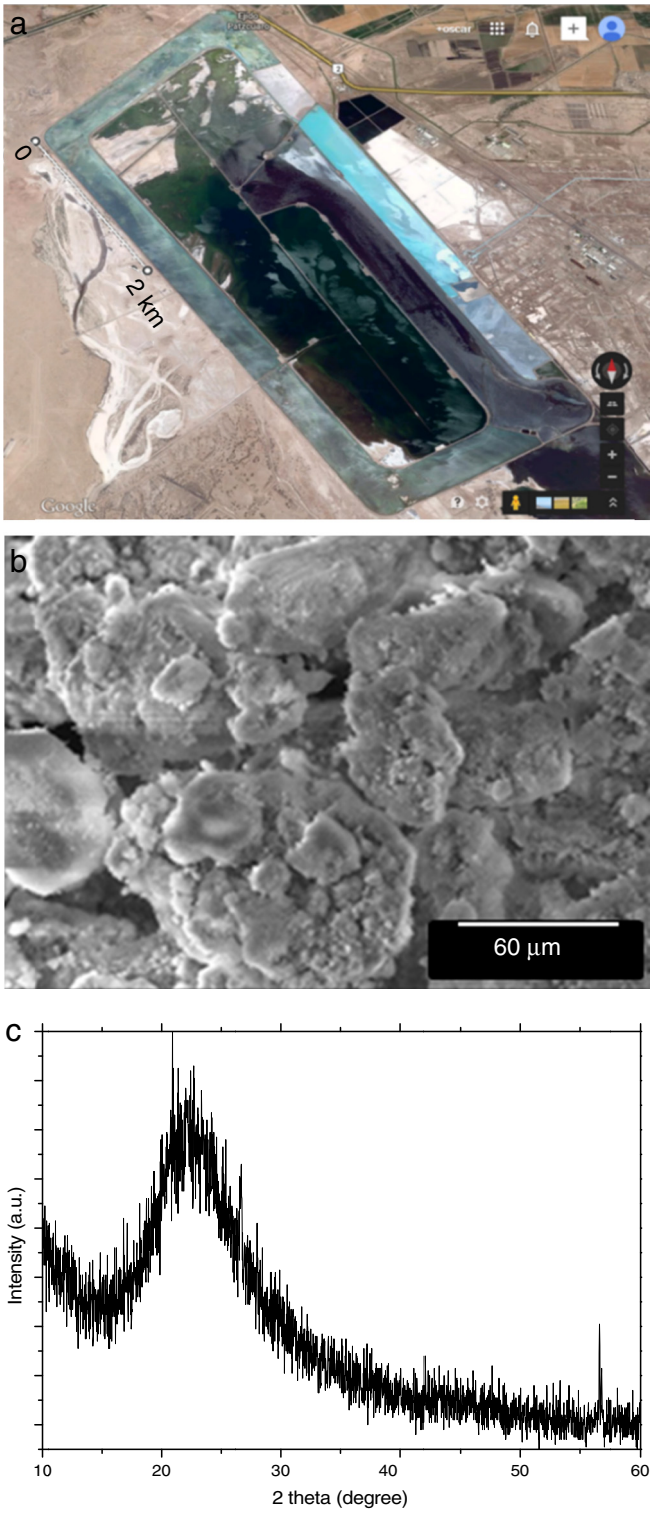

Fig. 1. (a) Aerial view of lagoon of mineralized waters at Cerro Prieto, Mexicali (INEGI-GOOGLE, 2015), (b) SEM image, and (c) DRX pattern of solid waste powders.

energy conversion solid waste materials by a solvent- and organic template-free process, with the inclusion of desired ion or ion combinations in a one step process leading to a series of materials with several potential applications. To demonstrate some of the potential applications, the use of [M]–S–MOR as photocatalyst is reported.

2. Materials and methods

Precursor SiO_2 powders (Fig. 1(b)) were obtained from geothermal energy conversion solid waste materials at Cerro Prieto plant.

Solid materials obtained from Cerro Prieto were cleaned by two mechanical wash processes, briefly, consist of mixing by stirring the solid residue obtained from the geothermal plant with deionized water, these washings are necessary to remove the clay that may have been mixed with the residue. X-ray diffraction (XRD) pattern analysis (Fig. 1(c)) revealed only an amorphous phase with the morphology shown in Fig. 1(b).

Elemental analysis by energy dispersive spectroscopy (EDS) confirmed the absence of any other element that could come from clays (Table 1).

Using this amorphous SiO_2 source, metal/mordenite ([M]–MOR) composites were synthesized with M = lithium, sodium, magnesium, titanium, chromium, manganese, iron, cobalt, nickel, copper, zinc, strontium, molybdenum, silver, cadmium, barium, lanthanum, gold, bismuth, and/or their mixtures, following the one-step route described in the MX/a/2012/013218 patent (Raymond, 2012). This process is solvent-, seed-, and organic template-free (avoiding the calcination processes to remove templates commonly used in the synthesis of zeolites), which involves 110 mL of a mixture of 0.1 M aqueous solutions of sodium silicate and aluminum sulfate (with SiO_2/Al_2O_3 molar relation of 15) that was stirred for 30 min; then, 30 mL of 0.1–0.3 M aqueous solution of desired ion salt was mixed with the first solution (this step is responsible to form nanoparticles in different concentrations). The final solution, with pH value of 9 ± 1, was autoclaved at 155 °C for 48 h. It eliminates the typical ion exchange process (to clarify, ion exchange is the most followed route to embed nanoparticles in silicon matrices, briefly, matrices were exposed to an concentrated solutions of the desired ion salt for at least 48 h then be washed) as it enables the inclusion of the desired ion (type and concentration) before the reaction. The possibility to select the ions before synthesis allows tuning the electro-optical properties and drastically reduces the obtaining time for this kind of materials because it does not require a calcination or evaporation process (Ren et al., 2012). The semiconductor/mordenite composites ([M]–S–MOR) are synthesized by exposure of the activated composites to an H_2S atmosphere for 24 h at room temperature.

Material composition, morphology and structure were studied by XRD with a Philips X'Pert diffractometer (CuKα radiation), by SEM using a JEOL JSM-5300 microscope with EDS attachment; by TEM with a JEOL JEM-2010 (with accelerating voltage of 200 kV), and by N_2 adsorption isotherms using a Tristar II 3020 Surface Area Analyzer. Optical properties were studied by UV–Vis spectroscopy using an AvaSpec-ULS2048-UA-50 spectrophotometer.

Table 1
Weight percent obtained by SEM–EDS chemical analysis and superficial area values from representative synthesized materials.

	Weight percent										
	Waste SiO_2	[Na]–MOR	[Mn]–MOR	[Fe]–MOR	[Ag]–MOR	[Ti,Ba,Sr]–MOR	[Cr,Ti,Fe]–MOR	[Ni, Co, Mo]–MOR	[Co,Mn]–S–MOR	[Cd,Zn,Ag]–S–MOR	[Cd,Zn]–S–MOR
O	33.2	51.8	51.3	51.3	44.9	49.3	48.4	50.4	50.3	50.8	49.9
Na	0	2.7	1.7	1.7	1.8	2.1	4.6	2.4	2.6	1.4	2.3
Al	0	5.5	4.4	5	3.8	4.4	3.9	4.9	4.0	4.7	5.0
Si	66.3	40.4	40.5	40	26.3	35.9	33.0	38.7	39.2	39.6	38.6
M	0	0	1	1	15	7.4	10.3	3.3	3.5	5.2	1.5
S	0	0	0	0	0	0	0	0	1	1	1.3
Si/Al	N/A	7	9	8	9	8	8	8	10	8	8
S.A.	1	328	240	275	210	247	185	301	83	74	101

S.A: superficial area (m^2/g).

3. Results and discussion

XRD patterns of all synthesized composites exhibit a defined single phase which matches well with the ICSD 68445 file reported for Na-mordenite; Figure 2 shows patterns of some [M]–MOR samples.

SEM and TEM analyses show the typical MOR morphology (Fig. 3), which consists of disc-shaped grains as arrangements of mordenite needle-like crystals. The SEM micrograph of sulfided [M]–S–MOR sample (Fig. 3(d), as representative case) shows the same morphology as [M]–MOR. The TEM micrograph (Fig. 3(e)) shows the general growth features of metal, semiconductor or metal/semiconductor nanoparticles (darker zones), strongly bonded to the mordenite matrix surface in all samples, which are homogeneously dispersed with an average size of 20 nm. Such features significantly increase the active surface required for multiple applications in catalysis, water treatments, and others (Liu et al., 2016; Mota, Eliášová, Jung, & Ryoo, 2016).

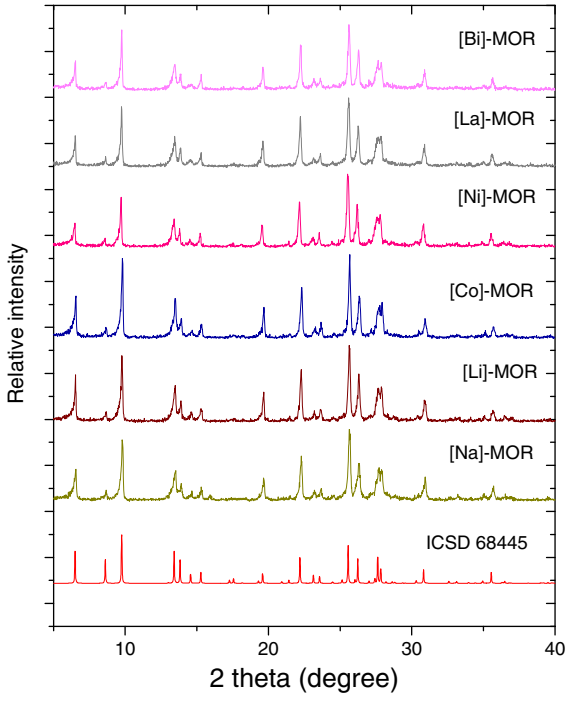

Fig. 2. XRD patterns of some synthesized mordenites compared with the ICSD 68445 file.

Table 1 summarizes the weight percent of each element for all materials and geothermal silica, obtained by EDS. An average value of 8.3 for the Si/Al ratio, obtained from EDS analysis, means that the mordenites have several acid sites used as cleavage centers for the nanoparticles; the particular ion at these acid sites determines the size of the nanoparticles. Fig. 4 shows a demonstrative scheme of the metal and/or semiconductor–mordenite composite. Situations A and B illustrate possible clusters grown inside the mordenite framework channels. The nanoparticles that grow outside the framework are strongly oriented by the Si–O–Al surface of the zeolite matrix.

Figure 5 shows a representative N_2 adsorption–desorption isotherm of the synthesized nanocomposite powders, which gives information about the micro- and mesoporosity structure and is closely related with the potential applications. Adsorption at very low partial pressures is associated with the zeolitic matrix micropore system (pore size < 2 nm), i.e., with the cavity and channel volumes inside the zeolite framework. Moreover, the N_2 adsorption extends at higher pressures, and a slight continuous slope at medium relative pressures arises from the N_2 adsorption on the external surface of the zeolite particles. An increase in the slope is also observed at high relative pressures ($P/P_0 > 0.8$), describing a hysteresis cycle, which indicates the presence of mesoporosity (pore size between 2 nm and 50 nm), i.e., the porosity generated on the composite surface and on the inter-crystallites volume inside the grains as can be seen in Figure 3.

From the N_2 adsorption–desorption isotherm analysis (Table 1) we found that the [M]–MOR samples have an average surface area of 240 m^2/g, while sulfided [M]–S–MOR composites showed a lower average surface area of 60 m^2/g.

On the other hand, UV–Vis spectroscopy results (Fig. 6(a)) revealed the optical-electronic properties for different metal composite samples. The [Na]–MOR spectrum was subtracted from all spectra. The spectra showed that the optical behavior of the [M]–MOR nanocomposites can be tuned depending on the kind of metal.

Below are listed potential applications for representative samples, derived from the results in the spectra of Fig. 6(a).

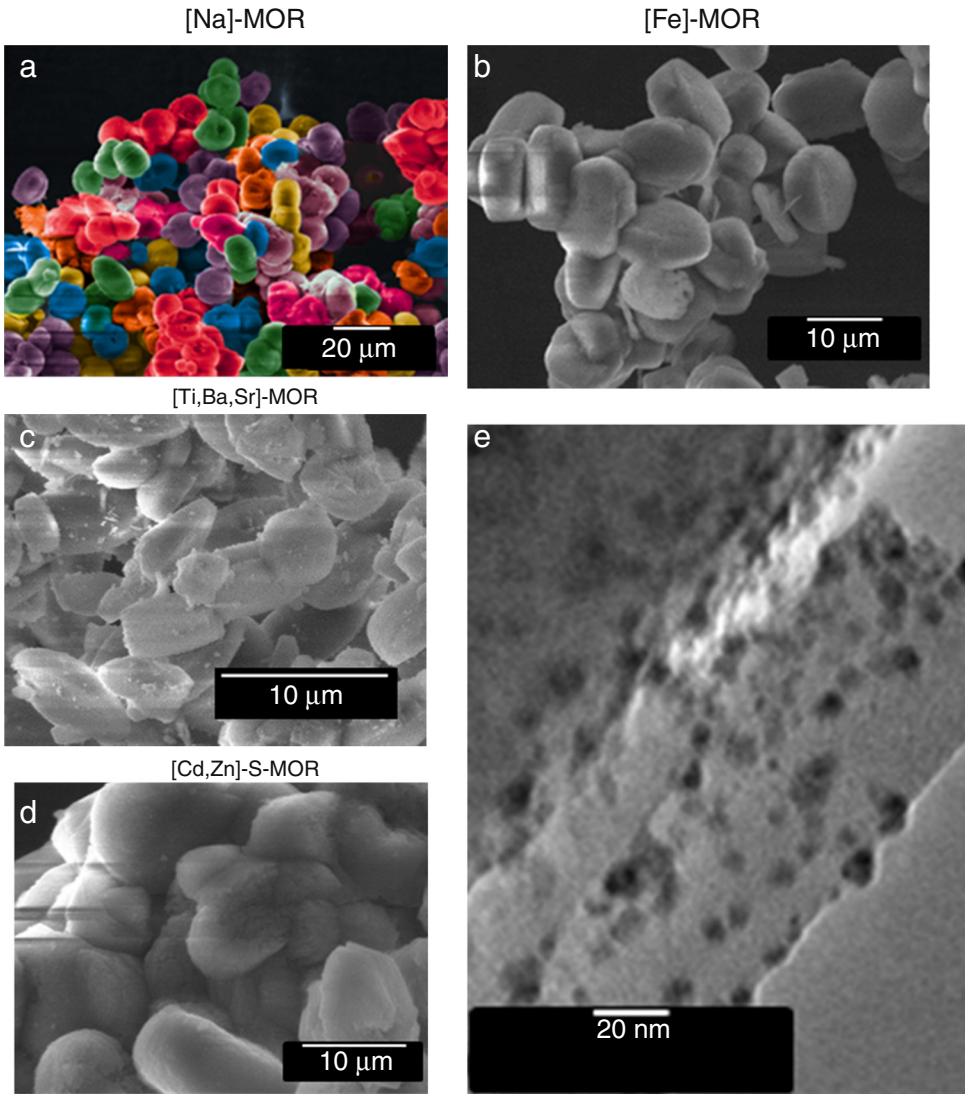

Fig. 3. (a–d) SEM and (e) TEM micrographs of representative samples.

A. For [Mn]–MOR two bands are evident, the band at ~500 nm is attributed to manganese coordination in Mn_3O_4 or MnO; the band at 250–270 nm is associated to ligand-to-metal charge-transfer transition on tetrahedral coordination (Azizi & Ehsani Tilami, 2013; Selvaraj et al., 2005). Such Mn signals are related to the coexistence of the 2+ and 4+ oxidation states and their intensity is attributed to the existence of coordination with Si. It is known that [Mn]–MOR composites are used in the production of methylamines (Hidaka, Higuchi, & Kawai, 2003), in the water oxidation process, and in hydrocarbon oxidation (Meng et al., 2013).

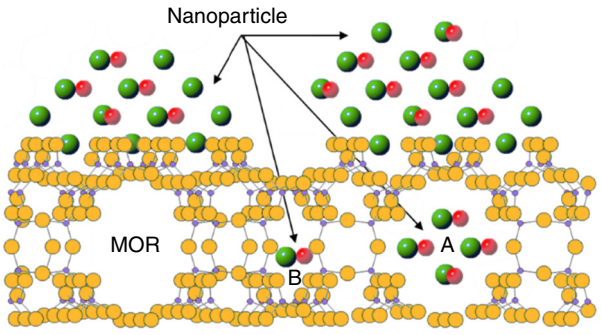

Fig. 4. Demonstrative scheme of the metal- and/or semiconductor nanoparticles grown inside and outside the mordenite framework.

B. The [Fe]–MOR sample displays a band at ~240 nm which may be attributed to metal–electron transfer transitions (Hailu et al., 2015). Moreover, a weak band at ~500 nm is related to high-spin tetrahedral complexes of Fe^{3+} (Fe_2O_3) (Hailu et al., 2015). [Fe]–MOR is suitable for Fenton treatments (Salazar, Brillas, & Sirés, 2012), in the oxidizing process on reformed gas (Watanabe, 2004), selective catalytic reduction on automotive emissions (Colombo, Koltsakis, Nova, & Tronconi, 2012), conversion of methane on methanol (Hammond et al., 2012), gasoline production by the Fischer–Tropsch reaction (Sun et al., 2012), among others.

C. For the [Co]–MOR sample, three bands appear at ~230, ~530 and ~635 nm; the two former transition bands correspond to Co^{2+} in octahedral coordination; while the transition at ~635 nm is due to tetrahedral of CoO_4 coordination present

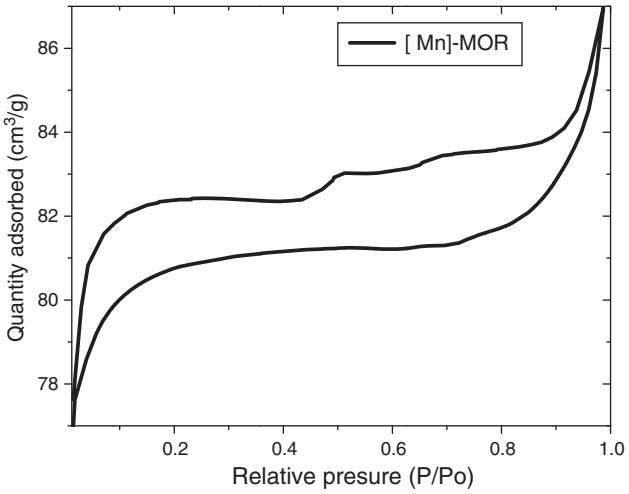

Fig. 5. Representative N_2 adsorption–desorption isotherm of synthesized [M]–MOR for M = Mn.

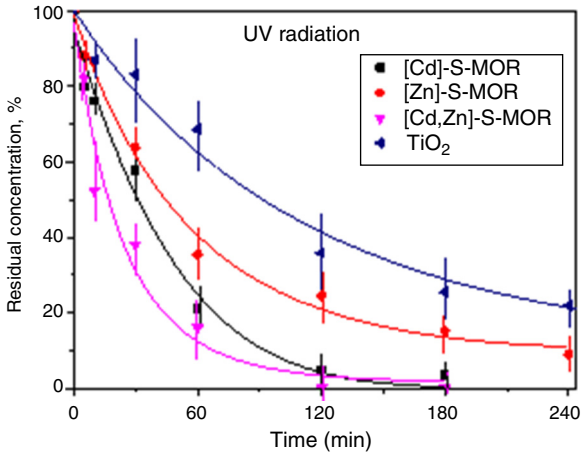

Fig. 7. AR114 dye photodegradation under UV radiation.

when Co substitutes Si atoms on the mordenite framework (Azizi & Ehsani Tilami, 2013; Kato, Ikeda, Kodaira, & Takahashi, 2011). [Co]–MOR is presently being used as a Fischer–Tropsch catalyst, to make liquid fuels from biosyngas (Sartipi et al., 2013).

D. For the [Ni]–MOR sample the absorbance around 700 nm is associated with the 2+ state of the Ni atoms. The absorbance between 270 and 300 nm may be related to octahedral coordinated Ni ions, surrounded by oxygen atoms of zeolite in electron–donor–acceptor complexes. [Ni]–MOR has been used for oligomerizations from propene for lubricants and detergents (Mlinar, Shylesh, Ho, & Bell, 2014), and conversion of cellulose to polyols such as sorbitol and mannitol (Shrotri, Tanksale, Beltramini, Gurav, & Chilukuri, 2012).

E. The [Cu]–MOR sample shows a transition band at 240 nm associated with Cu^{+}; the shoulder at ~500 nm is attributed to copper nanoparticles on the mordenite surface which corresponds to the capacity of copper to occupy acid sites on the mesoporosity. The signal at ~700 nm corresponds to the spin-allowed d–d transition of Cu^{2+} on zeolite matrices (López-Bastidas, Petranovskii, & Machorro, 2012). [Cu]–MOR is used in the carbonylation process for organic molecule production, oxidations of organic molecules to obtain phenol (Tabler, Häusser, & Roduner, 2013), and inactivation of viruses (Imai et al., 2012).

F. The [Ag]–MOR shows a typical absorbance spectrum associated to a plasmon resonance in the 340–530 nm region. [Ag]–MOR is used in pesticide degradation (Kanan & Nusri, 2013); in green chemistry, and in the production of important pharmacological molecules such as spiroketals (Borghèse, Drouhin, Bénéteau, Louis, & Pale, 2013).

Furthermore, the sulfided [M]–S–MOR UV–Vis absorbance spectra (Fig. 6(b)) show the modifications of the absorption spectrum for each example. These changes can be associated to the growth of sulfided nanoparticles as reported elsewhere (Jaime-Acuña et al., 2014). A noticeable increase of the sulfide samples absorption spectra is observed in the 225–550 nm range. This effect is due to the formation of semiconductor nanoparticles which are strongly photoactive and are responsible for the high yield of UV–Vis light harvesting. This type of nanocomposites were tested in the photocatalytic degradation of the organic molecules reaction (Eqs. (1)–(5)); briefly, a 20 ppm of some [M]–S–MOR nanocomposites and 50 ppm of acid red 114 (AR114) dye were stirred under UV light (254 nm). A commercial TiO_2 sample was used as reference. Fig. 7 shows the

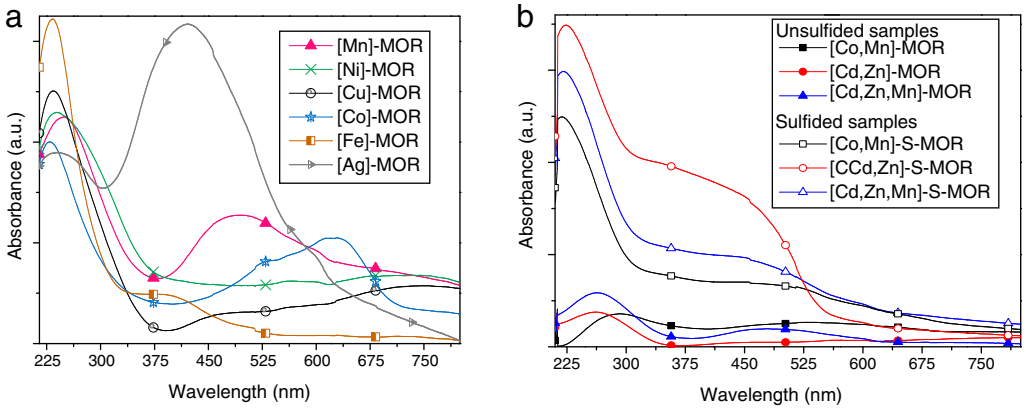

Fig. 6. UV–Vis spectra of (a) single metal nanocomposites, and (b) comparison between unsulfided and sulfided mixed metal composites.

residual concentration behavior of the AR114 dye as a function of time.

$$[\text{M}]\text{–S–MOR} + h\upsilon \rightarrow [\text{M}]\text{–S–MOR}(e_{BC}{}^{-} + h_{BV}{}^{+}) \quad (1)$$

$$[\text{M}]\text{–S–MOR}(h\upsilon_{BV}{}^{+}) + \text{H}_2\text{O} \rightarrow [\text{M}]\text{–S–MOR} + \text{H}^{+} + \text{OH}^{-} \quad (2)$$

$$[\text{M}]\text{–S–MOR}(h\upsilon_{BV}{}^{+}) + \text{OH}^{-} \rightarrow [\text{M}]\text{–S–MOR} + \text{OH}^{\bullet} \quad (3)$$

$$\text{O}_2{}^{\bullet-} + \text{H}^{+} \rightarrow \text{HO}_2{}^{\bullet} \quad (4)$$

$$\text{AR114} + \text{O}_2{}^{\bullet-} + \text{HO}_2{}^{\bullet} + \text{OH}^{\bullet} + \text{OH}^{-} \rightarrow \text{photodegradation} \quad (5)$$

As shown in Figure 7, while for the commercial TiO_2 the degradation reached ~75% in 215 min ($k = 0.004\ \text{min}^{-1}$), the [M]–S–MOR samples revealed a significantly better performance. The [Cd,Zn]–S–MOR sample shows the best performance with a degradation of ≥95% in only 100 min ($k = 0.009\ \text{min}^{-1}$), the explanation of the calculation of the reaction rate could be found elsewhere (Trejo-Tzab, Alvarado-Gil, Quintana, & Bartolo-Pérez, 2012). Thus, the [M]–S–MOR nanocomposites here developed exhibit higher photoactivity and better harvesting of the light making our products industrially competitive.

4. Conclusions

Waste solid materials, derived from the geothermal energy conversion process, were successfully used in solvent- and organic-free synthesis of nanostructured composites based on mordenite.

This route for synthesizing metal–MOR, semiconductor–MOR and metal/semiconductor–MOR nanostructured composites has the following advantages: (i) reduction of pollutants (no solvents are used); (ii) saving energy and simplifying synthetic procedures (no organic templates are used which means no calcination process is required); (iii) designation of the type and concentration of ion supported on MOR from the beginning of the synthesis. With these considerations, the proposed synthesis route becomes relevant for the industrial production of nanostructured composites based on synthetic zeolite.

The developed methodology allows control and tuning of the final properties of nanocomposites from their synthesis in addition to being reproducible and repeatable. Metal–semiconductor– and metal/semiconductor–MOR nanostructured composites could be widely used in industry and are strong candidates as materials for new developments in optoelectronics, catalysis, and especially in photocatalysis.

Conflict of interest

The authors have no conflicts of interest to declare.

References

Ambec, S., Cohen, M. A., Elgie, S., & Lanoie, P. (2013). The Porter hypothesis at 20: Can environmental regulation enhance innovation and competitiveness? *Review of Environmental Economics and Policy*, http://dx.doi.org/10.1093/reep/res016, res016

Azizi, S. N., & Ehsani Tilami, S. (2013). Framework-incorporated Mn and Co analcime zeolites: Synthesis and characterization. *Journal of Solid State Chemistry*, *198*, 138–142. http://dx.doi.org/10.1016/j.jssc.2012.10.001

Bibby, D. M., & Dale, M. P. (1985). Synthesis of silica–sodalite from non-aqueous systems. *Nature*, *317*(6033), 157–158. http://dx.doi.org/10.1038/317157a0

Borghèse, S., Drouhin, P., Bénéteau, V., Louis, B., & Pale, P. (2013). Silver–zeolite catalysed solvent free synthesis of (spiro)ketals. *Green Chemistry*, *15*(6), 1496. http://dx.doi.org/10.1039/c3gc40422f

Colombo, M., Koltsakis, G., Nova, I., & Tronconi, E. (2012). Modelling the ammonia adsorption–desorption process over an Fe–zeolite catalyst for SCR automotive applications. *Catalysis Today*, *188*(1), 42–52. http://dx.doi.org/10.1016/j.cattod.2011.09.002

Cooper, E. R., Andrews, C. D., Wheatley, P. S., Webb, P. B., Wormald, P., & Morris, R. E. (2004). Ionic liquids and eutectic mixtures as solvent and template in synthesis of zeolite analogues. *Nature*, *430*(7003), 1012–1016. http://dx.doi.org/10.1038/nature02860

Hailu, S. L., Nair, B. U., Redi-Abshiro, M., Aravindhan, R., Diaz, I., & Tessema, M. (2015). Synthesis, characterization and catalytic application of zeolite based heterogeneous catalyst of iron (III), nickel (II) and copper (II) salen complexes for oxidation of organic pollutants. *Journal of Porous Materials*, *22*(5), 1363–1373. http://dx.doi.org/10.1007/s10934-015-0015-9

Hammond, C., Forde, M. M., Ab Rahim, M. H., Thetford, A., He, Q., Jenkins, R. L., et al. (2012). Direct catalytic conversion of methane to methanol in an aqueous medium by using copper-promoted Fe–ZSM-5. *Angewandte Chemie – International Edition*, *51*(21), 5129–5133. http://dx.doi.org/10.1002/anie.201108706

Hidaka, T., Higuchi, K., & Kawai, T. (2003). United States Patent, 6590124.

Imai, K., Ogawa, H., Bui, V. N., Inoue, H., Fukuda, J., Ohba, M., et al. (2012). Inactivation of high and low pathogenic avian influenza virus H5 subtypes by copper ions incorporated in zeolite–textile materials. *Antiviral Research*, *93*(2), 225–233. http://dx.doi.org/10.1016/j.antiviral.2011.11.017

INEGI-GOOGLE, www.google.com/maps?q=geotermica+de+cerro+prieto (accessed 06.15.15).

Jaime-Acuña, O. E., Villavicencio, H., Díaz-Hernández, J. A., Petranovskii, V., Herrera, M., & Raymond-Herrera, O. (2014). Atomic and electronic structure of quaternary CdxZnySδOγ nanoparticles grown on mordenite. *Chemistry of Materials*, *26*, 6152–6159. http://dx.doi.org/10.1021/cm5024585

Kanan, S. M., & Nusri, S. E. (2013). The effect of silver and silver–platinum doped into 5A zeolite on the degradation of naptalam. *Advanced Materials Research*, *856*, 43–47. http://dx.doi.org/10.4028/www.scientific.net/AMR.856.43

Kato, M., Ikeda, T., Kodaira, T., & Takahashi, S. (2011). Synthesis of Co-substituted zeolites in the presence of cobalt complex with EDMA. *Microporous and Mesoporous Materials*, *142*(2–3), 444–453. http://dx.doi.org/10.1016/j.micromeso.2010.12.030

Liu, S., Ren, J., Zhang, H., Lv, E., Yang, Y., & Li, Y. W. (2016). Synthesis, characterization and isomerization performance of micro/mesoporous materials based on H-ZSM-22 zeolite. *Journal of Catalysis*, *335*, 11–23.

López-Bastidas, C., Petranovskii, V., & Machorro, R. (2012). Optical response of Cu clusters in zeolite template. *Journal of Colloid and Interface Science*, *375*(1), 60–64. http://dx.doi.org/10.1016/j.jcis.2012.02.036

Meng, Y., Genuino, H. C., Kuo, C. H., Huang, H., Chen, S. Y., Zhang, L., et al. (2013). One-step hydrothermal synthesis of manganese-containing MFI-type zeolite, Mn–ZSM-5, characterization, and catalytic oxidation of hydrocarbons. *Journal of the American Chemical Society*, *135*(23), 8594–8605.

Mlinar, A. N., Shylesh, S., Ho, O. C., & Bell, A. T. (2014). Propene oligomerization using alkali metal- and nickel-exchanged mesoporous aluminosilicate catalysts. *ACS Catalysis*, *4*(1), 337–343. http://dx.doi.org/10.1021/cs4007809

Mota, F. M., Eliášová, P., Jung, J., & Ryoo, R. (2016). Mesoporous EU-1 zeolite as a highly active catalyst for ethylbenzene hydroisomerization. *Catalysis Science & Technology*, *6*(8), 2735–3274.

Raymond, O. (2012). *Mexico patent*. , http://lp.espacenet.com/publicationDetails/originalDocument?CC=MX&NR=2012013218A&KC=A&FT=D&ND=4&date=20140522&DB=lp.espacenet.com&locale=es_LP.

Ren, L., Wu, Q., Yang, C., Zhu, L., Li, C., Zhang, P., et al. (2012). Solvent-free synthesis of zeolites from solid raw materials. *Journal of the American Chemical Society*, *134*(37), 15173–15176. http://dx.doi.org/10.1021/ja3044954

Salazar, R., Brillas, E., & Sirés, I. (2012). Finding the best Fe^{2+}/Cu^{2+} combination for the solar photoelectro-Fenton treatment of simulated wastewater containing the industrial textile dye Disperse Blue 3. *Applied Catalysis B: Environmental*, *115-116*, 107–116. http://dx.doi.org/10.1016/j.apcatb.2011.12.026

Sartipi, S., Alberts, M., Meijerink, M. J., Keller, T. C., Pérez-Ramírez, J., Gascon, J., et al. (2013). Towards liquid fuels from biosyngas: Effect of zeolite structure in hierarchical-zeolite-supported cobalt catalysts. *ChemSusChem*, *6*(9), 1646–1650. http://dx.doi.org/10.1002/cssc.201300339

Selvaraj, M., Sinha, P. K., Lee, K., Ahn, I., Pandurangan, A., & Lee, T. G. (2005). Synthesis and characterization of Mn–MCM-41 and Zr–Mn–MCM-41. *Microporous and Mesoporous Materials*, *78*(2–3), 139–149. http://dx.doi.org/10.1016/j.micromeso.2004.10.004

Shrotri, A., Tanksale, A., Beltramini, J. N., Gurav, H., & Chilukuri, S. V. (2012). Conversion of cellulose to polyols over promoted nickel catalysts. *Catalysis Science & Technology*, *2*(9), 1852. http://dx.doi.org/10.1039/c2cy20119d

Sun, B., Yu, G., Lin, J., Xu, K., Pei, Y., Yan, S., et al. (2012). A highly selective Raney Fe@HZSM-5 Fischer–Tropsch synthesis catalyst for gasoline production: One-pot synthesis and unexpected effect of zeolites. *Catalysis Science & Technology*, *2*(8), 1625. http://dx.doi.org/10.1039/c2cy20155k

Tabler, A., Häusser, A., & Roduner, E. (2013). Aerobic one-step oxidation of benzene to phenol on copper exchanged HZSM5 zeolites: A mechanistic study. *Journal of Molecular Catalysis A: Chemical*, *379*, 139–145. http://dx.doi.org/10.1016/j.molcata.2013.08.012

Trejo-Tzab, R., Alvarado-Gil, J. J., Quintana, P., & Bartolo-Pérez, P. (2012). N-doped TiO_2 P25/Cu powder obtained using nitrogen (N_2) gas plasma. *Catalysis Today*, *193*(1), 179–185.

Watanabe, M. (2004). United States Patent, 6726890.

Zaarour, M., Dong, B., Naydenova, I., Retoux, R., & Mintova, S. (2014). Progress in zeolite synthesis promotes advanced applications. *Microporous and Mesoporous Materials*, *189*, 11–21. http://dx.doi.org/10.1016/j.micromeso.2013.08.014